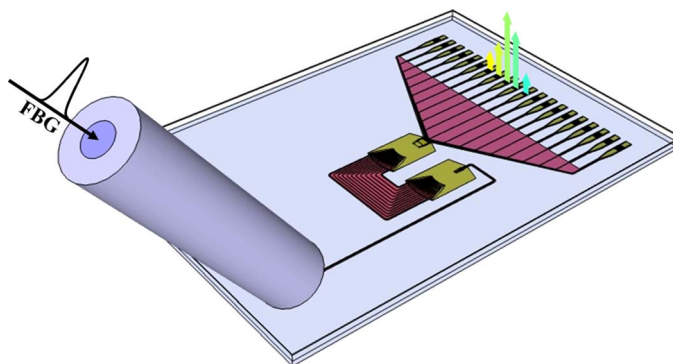


# Simultaneous Interrogation of Multiple Fiber Bragg Grating Sensors Using an Arrayed Waveguide Grating Filter Fabricated in SOI Platform

Volume 7, Number 6, December 2015

Andrea Trita  
Eli Voet  
Jan Vermeiren  
Danae Delbeke  
Pieter Dumon  
Shibnath Pathak  
Dries Van Thourhout



DOI: 10.1109/JPHOT.2015.2499546  
1943-0655 © 2015 IEEE

# Simultaneous Interrogation of Multiple Fiber Bragg Grating Sensors Using an Arrayed Waveguide Grating Filter Fabricated in SOI Platform

Andrea Trita,<sup>1,4</sup> Eli Voet,<sup>2</sup> Jan Vermeiren,<sup>3</sup> Danae Delbeke,<sup>1</sup> Pieter Dumon,<sup>1</sup> Shibnath Pathak,<sup>1</sup> and Dries Van Thourhout<sup>1</sup>

<sup>1</sup>Photonics Research Group, Department of Information Technology (INTEC), IMEC–Ghent University, 9000 Ghent, Belgium

<sup>2</sup>Department of Materials Science and Engineering, Ghent University, 9052 Ghent, Belgium

<sup>3</sup>Xenics nv, 3001 Leuven, Belgium

<sup>4</sup>Rockley Photonics, Inc., Pasadena, CA 91101 USA

DOI: 10.1109/JPHOT.2015.2499546

1943-0655 © 2015 IEEE. Translations and content mining are permitted for academic research only.

Personal use is also permitted, but republication/redistribution requires IEEE permission.

See [http://www.ieee.org/publications\\_standards/publications/rights/index.html](http://www.ieee.org/publications_standards/publications/rights/index.html) for more information.

Manuscript received October 13, 2015; revised November 1, 2015; accepted November 3, 2015. Date of publication November 11, 2015; date of current version November 23, 2015. This work was supported by the European Commission under the Seventh Framework Program through the SMARTFIBER (257733) project. Corresponding author: A. Trita (e-mail: andrea.trita@unipv.it).

**Abstract:** A novel fiber Bragg grating (FBG) interrogator is demonstrated based on an optimized arrayed waveguide grating (AWG) filter. The AWG response is optimized to achieve large crosstalk between the output channels, which allows simultaneous detection of multiple FBG peaks, using centroid signal processing techniques, without constraints on the minimum FBG peak spectral width. The measured interrogator resolution is 2.5 pm, and the total measurement range is 50 nm. The device is fabricated in a silicon-on-insulator platform and has a footprint of only  $2.2 \times 1.5$  mm. A novel approach to minimize the polarization dependence of the device is proposed and experimentally demonstrated.

**Index Terms:** Integrated optics devices, wavelength filtering devices, remote sensing and sensors.

## 1. Introduction

In recent years, structural health monitoring (SHM) of composite structures in service has attracted a great deal of attention as it allows operation of the composite structures much closer to their design limits, providing, at the same time, increased safety margins. Fiber Bragg Grating sensors (FBGs) are an appealing solution for SHM of composite structures as they offer several advantages such as compactness, light weight, immunity to electromagnetic interferences (EMI), high resistance to corrosion, and a large operating temperature range. They can be multiplexed, allowing strain measurement at multiple locations along a single fiber line, and additionally, during fabrication of the composite, the FBGs fibre can be embedded in between the reinforcement fibres, causing negligible distortion of the composite structure, especially if the optical fibre has a small diameter [1]. Numerous solutions for miniaturized FBG wavelength interrogation have been reported in literature so far, based on scanning Fabry–Pérot interferometers [2], Mach–Zehnder

interferometer [3], charge-coupled device spectrometers [4], and discriminators using the power ratio of optical filters [5], scanning lasers [6], and Arrayed Waveguide Grating (AWG) filters [7]–[12].

FBG interrogators based on AWG filters offer multiple advantages with respect to other interrogation schemes, specifically compact size and stability due to the monolithic nature of the component, potential for high-speed interrogation [12], they allow for integration of other functionalities on the same chip (e.g., detectors, signal processing, and controlling electronics, etc.), and they can be manufactured in large volumes. Several FBG interrogation schemes based on AWG filters have been reported in literature [7]–[12]. In [7] an FBG interrogator has been proposed based on the detection of the power ratio between the transmitted signals by two adjacent AWG channels. This technique provides high accuracy and allows measuring several FBGs simultaneously. However the measurement range for each FBG is limited to the small wavelength interval where the two neighboring AWG channels cross each other, and the measurement sensitivity drops considerably at the edges of the measurement band [12]. In order to extend the measurement range in [10] and [11] it has been proposed to measure the powers of more than two AWG channels. Main drawback of this technique is that it requires that the FBG peak overlaps several AWG channels, thus imposing a trade-off between the AWG channel spacing and the minimum FBG peak spectral width.

In this paper, we report an FBG interrogator based on an optimized AWG filter, which allows simultaneous interrogation of multiple FBGs with high resolution and uniform sensitivity on a broad measurement range, without any constraint on the minimum FBG peak spectral width. The spectral response of the AWG filter is optimized such to achieve intentional large cross-talk between the AWG channels, which allows the FBG peak under test to produce a detectable output signal over several channels. By means of centroid signal processing techniques it is then possible to track the position of the FBG with an accuracy much higher than the AWG channel spacing.

The AWG is implemented in a SOI platform; thus, it offers the potential advantage of large scale fabrication and cost reduction associated to the well-established industrial infrastructure of silicon-based microfabrication. The high index contrast of the SOI platform allows pushing the miniaturization of the interrogator to an extent that is not achievable using standard platforms (e.g., Silica). This can lead to low-cost SOI photonic chips with multiple interrogators onboard, capable of simultaneous read-out of a very large number of FBG sensors.

One of the best examples reported so far in the literature [8] of an FBG interrogator in the SOI platform, based on an AWG filter, features a resolution of 1.8 pm and a total measurement bandwidth of 9 nm. This remarkable result is achieved by exploiting a high-resolution SOI AWG spectrometer as interrogation circuit. The AWG spectrometer features a very small channel spacing of 0.18 nm but the free-spectral-range (which in turn sets the total measurement bandwidth of the FBG interrogator) is limited to 9 nm. In our work, by optimizing the AWG response, we are able to achieve a comparable high resolution (5 pm) but on a much larger total measurement bandwidth (50 nm).

One major concern associated with the SOI nanophotonics platform is the large structural birefringence, which can lead to polarization mode dispersion (PMD), polarization dependent loss (PDL), and polarization-dependent wavelength characteristics ( $PD\lambda$ ), and therefore, SOI photonic circuits are usually designed to work only for one specific polarization. A common way to solve this problem is to exploit a full polarization diversity approach [13]–[15] consisting of polarization splitters and rotators. The TE and TM components are separated by the splitter, and the TM component is rotated  $90^\circ$  by the rotator. The two TE polarized signals are then processed by two identical replicas of the original chip designed for TE polarization. At the output, a copy of the polarization rotator and splitter are implemented in order to combine the two polarizations without interference. To enable this approach several integrated polarization rotators and splitters have been demonstrated over the years [13]–[17]. Alternatively 2-D grating couplers (2D-GC) can be exploited as they [18] naturally incorporate the splitting and rotating functionality, in addition to coupling to an external optical fiber, and thus are ideally suited for the implementation of a polarization diversity circuit. With the reflection from the FBG sensor randomly

polarized, if no countermeasures are applied, our interrogator would suffer both large PDL and  $PD\lambda$ . For this reason, we devised two novel polarization diversity approaches based on 2-D grating couplers. The first approach, very similar to the conventional polarization diversity scheme described above, features 2D-GCs at the input, two identical replicas of the AWG interrogator and 1-D grating couplers at the output of the two AWGs. Using 1D-GCs at the output instead of 2D-GCs (and thus not recombining the two orthogonal polarization at the end as in conventional polarization diversity approaches) allows to monitor the two orthogonal polarization individually. This feature can be conveniently exploited to perform multi-axial strain measurement with Fiber Bragg Gratings inscribed in birefringent optical fibers [19]. The second proposed approach exploits again a 2D-GC as input interface. The two TE polarized signals from the 2D-GC are subsequently transmitted by a Mach–Zehnder interferometer in which one of the two arms is longer than the coherence length of the signal reflected by the FBG, and finally the resulting signal is processed by a single AWG interrogator. The arm length difference being longer than the coherence length of the signal, no interference effects will be observed at the output of the 3 dB combiner. Thus, independently of the polarization status, the input signal is transformed into a TE signal (albeit at the expense of an additional fixed 3 dB loss), which is then processed by a single AWG interrogator. This novel approach, although resulting in a fixed additional 3 dB loss, allows minimization of the PDL of the device (as experimentally reported in the last section of this paper), has the advantage of simplicity, reduced footprint, and it is not susceptible to the unavoidable fabrication tolerances between the two identical replicas of the photonic circuit as needed in the conventional polarization diversity approach.

## 2. Theory

The proposed FBG interrogator is based on an arrayed waveguide grating filter. An AWG is a device that can separate (or combine) signals at different wavelength. Conversely to a conventional AWG designed for Wavelength Division Multiplexing based optical networks where low adjacent channel crosstalk is sought, the AWG investigated in this paper features an intentional large but controlled crosstalk between the channels, which allows the FBG peak under test to produce a measurable output signal over several output channels when transmitted by the AWG [see Fig. 1(c)]. Prior knowledge of the AWG channel position  $\lambda_{CH,i}$ , combined with power values transmitted by the AWG channels  $P_{CH,i}(\lambda_{FBG})$ , allows estimation of the center of mass of the FBG peak under test [see Fig. 1(d)] using the Center Of Gravity (CoG) detection technique [20]:

$$\lambda_{FBG} = \frac{\sum_i P_{CH,i}(\lambda_{FBG}) \cdot \lambda_{CH,i}}{\sum_i P_{CH,i}(\lambda_{FBG})} \quad (1)$$

An AWG [21], [22] is composed of two free propagation regions (FPRs) that are designed to provide focusing functionality, connected together by an array of waveguides featuring a constant incremental optical path difference, which is equal to an integer multiple of the center wavelength of the demultiplexer  $\lambda_c$ . Light diffracted from the input port, after travelling the first FPR, is coupled into the array of waveguides and then further propagates through the second FPR, finally reaching the output port. For the center wavelength  $\lambda_c$  the optical fields travelling through the different waveguides of the dispersive array arrive at the output aperture with equal phase and thus the field distribution at the output aperture is a replica of the field at the input aperture. For  $\lambda \neq \lambda_c$  the increasing length of the waveguides results in a linear phase change across their outputs. This phase delay induces a tilt in the phase fronts propagating in the second FPR and thus a shift of the focal point along the image plane. By proper positioning the receiver waveguides along the image plane, spatial separation of the input wavelengths is achieved.

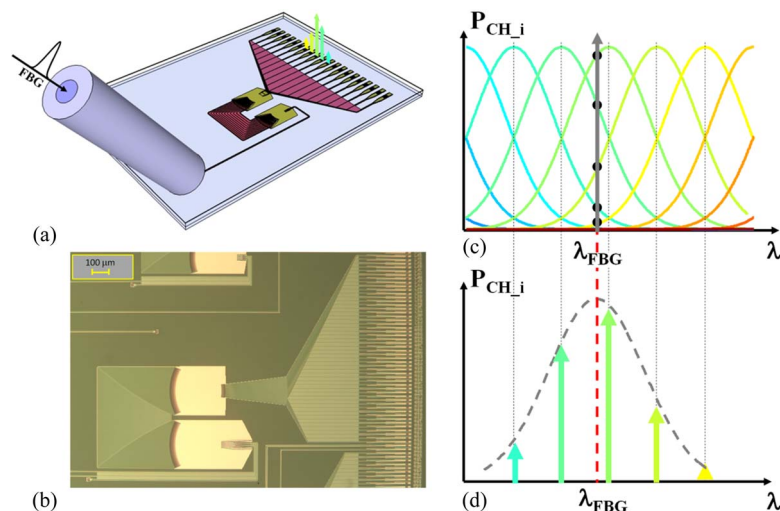


Fig. 1. Operating principle of the interrogator. (a) Sketch of the device. (b) Optical microscope image of the fabricated device. The total footprint is  $2.2 \times 1.5$  mm. (c) The FBG peak produces a measurable output over several channels. (d) The center of mass of the FBG peak can be estimated using the recorded power values if the AWG channel positions are known.

The spectral response of the AWG channels is determined by the overlap of the shifted field profile with the mode profile of the different output waveguide located at the image plane. In conventional AWG design the input and output aperture waveguides have the same cross section. This results in maximal overlap (and thus low insertion losses) when the field on the image plane is aligned with one of the output waveguide apertures and steep roll off of the channel response for small wavelength deviations with respect to the corresponding center wavelength of the channel. This in turn implies a very small cross talk between adjacent channels, which is highly favorable in the case of (de)multiplexer applications for example, where a sharp separation of the input spectrum is desired. For our application, as explained above, a large crosstalk between the AWG channels is sought. One way to achieve this result is to reduce the distance between the output waveguides on the image plane. This approach, however, proves to be not very successful as there is a physical limit to the minimum distance between the output waveguides, and little channel spectral superposition can be achieved, especially for non-nearest neighboring channels. To attain the required large superposition we designed the device with different input/output waveguide apertures. In particular a larger waveguide aperture is used at the input side with respect to the output side. As a consequence, a large image is produced on the output focal plane, overlapping several receiver waveguides and providing the required channel superposition. This result, of course, comes at the expense of a reduced peak channel transmission (as the input signal is now partly transmitted through the neighboring overlapping channels).

### 3. Design and Fabrication of the Device

The device [see Fig. 1(b)] is fabricated on a 200 mm Silicon on Insulator (SOI) wafer featuring a 220 nm Si slab on top of a 2  $\mu\text{m}$  buried oxide layer (BOX). The patterns are defined using 193 nm deep UV lithography in combination with a double etch process. A deep 220 nm etch is used to define high confinement photonic wires. A shallow 70 nm etch is used to define the grating couplers for IN/OUT coupling of the chip and to define the low contrast waveguides interfacing with the star coupler regions. Low contrast waveguides are used at the star-coupler interfaces such to reduce reflections in the transition zone [23]. To cover the 50 nm target measurement range for the FBG interrogator, the AWG is designed with 50 channels spaced by 1 nm. The set free spectral range is also 50 nm, thus the device operates as a router. An array of 150 waveguides, tapered to 2  $\mu\text{m}$  at the star coupler interfaces, and spaced by 0.2  $\mu\text{m}$ , connects the two FPR. The input waveguide,

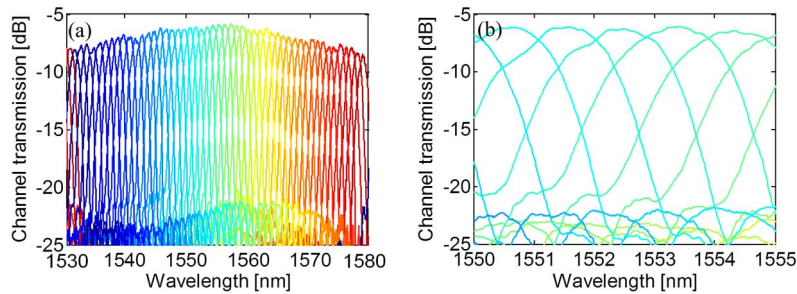


Fig. 2. Measured spectral response of the device. (a) Full spectral order. (b) Detail of the spectral response around the center wavelength. Large intentional cross-talk between the channels is achieved.

i.e., a 450 nm wide photonic wire, is tapered to 5  $\mu\text{m}$  using a 200  $\mu\text{m}$  long adiabatic taper before reaching the first FPR. At the exit of the second FPR, shallow waveguides with 1  $\mu\text{m}$  aperture are used, which are connected to the output waveguides (again 450 nm wide photonic wires) using a 25  $\mu\text{m}$  long adiabatic taper. An input/output aperture width ratio of 5 is thus set, which ensures that the image of the input aperture on the focal plane overlaps several output waveguides.

The spectral response of the fabricated device, measured using a tunable laser source, is shown in Fig. 2. Large intentional cross talk between the output channels of the AWG is observed. In particular, for the center channel, the measured first and the second neighbor channel crosstalk are respectively  $-2.8$  dB and  $-12.5$  dB, and the measured 3 dB and 10 dB pass-band widths are, respectively, 1.84 and 2.98 nm. The peak transmission of the center AWG channel is in the order of  $-6$  dB, hence, as expected, lower than in conventional designs, however still largely acceptable for our application. The noise floor level, mostly set by the phase noise introduced by the waveguide array, is around  $-15$  dB below the peak channel transmission, thus an adequate dynamic range is achieved. From the measured spectral response we estimated the center of mass of each AWG channel. These values will be required later, in order to apply the CoG formula (1) to estimate the FBG peak position.

## 4. Experimental Results

### 4.1. Experimental Set-Up

A sketch of the experimental set-up used to characterize the FBG interrogator is shown in Fig. 3. Light emitted from a broadband source (a Super Luminescent Diode, center wavelength = 1550 nm, 3 dB pass-band width = 55 nm) is coupled to the FBG fiber under test using an optical circulator. One end of the FBG fiber is clamped to the optical table, while the other one is clamped to a micrometric translation stage which allows applying a controlled strain to the sensor fiber. The FBG under test is a draw tower grating (DTG) manufactured by FBGS international. The FBG features a peak reflection of  $-7$  dB around 1557 nm, a peak FWHM of 120 pm and a strain sensitivity of  $7.8 \mu\text{m}^{-1} \times 10^{-7}$ . The reflection from the FBG is split in two: half of the signal is sent to a commercial interrogator (FBG-scan608 from FOS&S with operational range between 1525–1565 nm and 1 pm resolution) used as a reference, and the other half is coupled to the device under test through an input 1-D grating coupler [24] using an SMF optical fiber. The device is mounted on a thermally stabilized sub-mount, such to avoid thermally induced wavelength shift of the AWG spectral response during the measurement. A variable optical attenuator (VOA) and a polarization controller (PC) are inserted before the SMF fiber to control the input power level to the device and to optimize the input polarization impinging on the input grating coupler. The output waveguides of the AWG are connected to an array of 1-D grating couplers which allow coupling the signal transmitted by the AWG out of the optical chip. The array of grating couplers is imaged by means of a large working distance 10 $\times$  optical objective followed by an Infrared Camera (model Xeva-1.7-320 manufactured by Xenics). An example

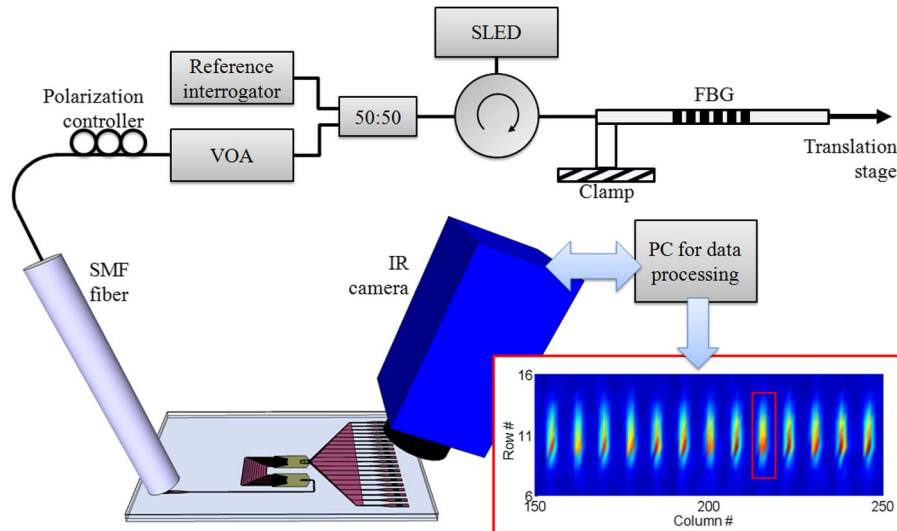


Fig. 3. Experimental set-up. (Inset) Image recorded by the IR camera when the broadband spectrum is directly transmitted by the AWG.

of the image acquired when the broadband spectrum is directly transmitted through the AWG is shown in the inset of Fig. 3. The array of grating couplers is clearly distinguishable. By integrating the recorded intensity over the grating coupler areas it is possible to deduce the optical power transmitted through each channel.

#### 4.2. Single FBG Interrogation

In order to demonstrate the operation of the proposed device as FBG interrogator the following experiment has been carried out. A controlled strain is applied to the FBG fiber under test in steps of  $25 \mu\epsilon$  by means of the translation stage, and the corresponding AWG channel outputs are recorded. At the same time the wavelength position of the FBG peak is measured using the commercial interrogator. The evolution of the AWG response as a function of the applied strain/FBG peak position is shown in Fig. 4(a). The FBG produces a significant signal over three to four AWG channels at any moment.

For each value of applied strain, the FBG peak position is then estimated by means of the CoG formula (1), using the measured AWG output values and the centers of mass of the AWG channels previously calculated. The result of this operation is shown in Fig. 4(b) (red line). A smooth relationship between the measured peak position and the applied strain is achieved, however the values predicted using the CoG formula differ slightly (always less than 50 pm) from the data measured using the commercial interrogator. The difference stems from the fact that the CoG formula gives exact results only if all the channels have exactly the same spectral shape and the spacing amongst them is constant, conditions that are not fulfilled by our device. The transfer function  $\lambda_{\text{CoG}}(\epsilon_i)$  estimated using the CoG formula, however, can be easily linearized using the correct peak positions  $\lambda_{\text{CI}}(\epsilon_i)$  which were measured simultaneously by means of the Commercial Interrogator. Indeed, a relation  $\lambda_{\text{CI}}(\lambda_{\text{CoG}})$  can be derived that can be used as “correction” function to apply to the data estimated using the CoG formula.

The accuracy of the “corrected” transfer function  $\lambda_{\text{FBG}}(\epsilon_i)$  is tested on a new set of 25 random points within the calibration range [see Fig. 4(c)]. The amplitude of the FBG peak, input to the device, is changed during the measurements, in order to investigate also the dynamic range of the device. The absolute difference between the FBG peak positions  $\lambda_{\text{FBG}}(\epsilon_i)$  calculated using the CoG formula and corrected using the “correction” function, and the FBG peak positions measured using the commercial interrogator  $\lambda_{\text{CI}}(\epsilon_i)$  turns out to be always less than 6 pm (on average is 2 pm), within a dynamic range of 10 dB.

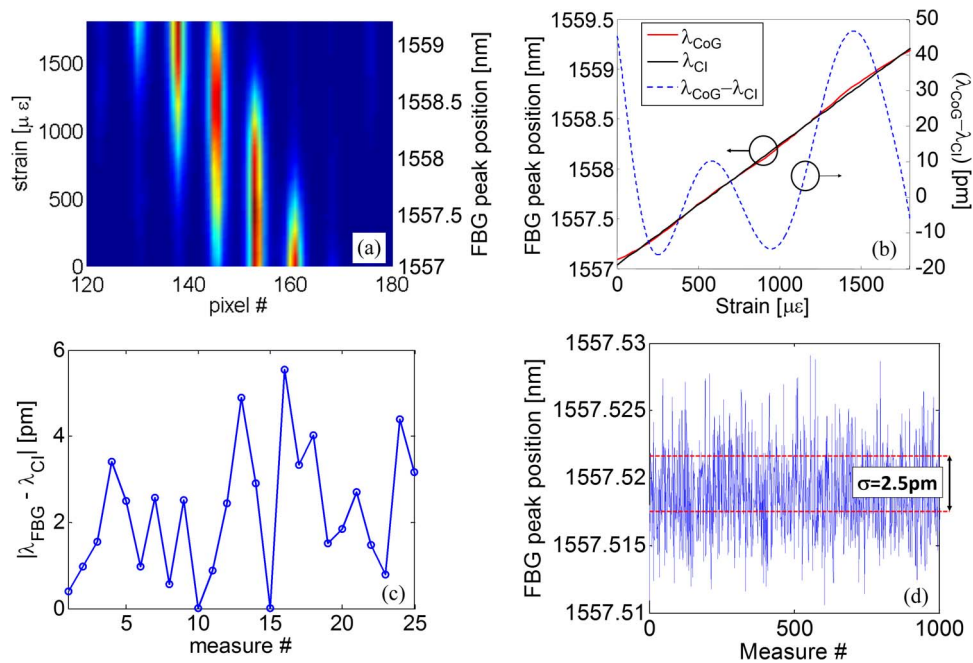


Fig. 4. (a) Evolution of the AWG response as a function of the applied strain/FBG peak position. (b) FBG peak position estimated using the CoG (red line), FBG peak position measured using the commercial interrogator (black line), and difference between the FBG peak position estimated using the and the FBG peak position measured using the commercial interrogator (dashed blue line), as a function of the applied strain. (c) Absolute difference between the FBG peak positions calculated using the CoG formula and corrected using the “correction” function and the FBG peak positions measured using the commercial interrogator for a set of 25 random points within the calibration range. (d) Fluctuations in the peak position calculated using the CoG formula and corrected using the “correction” function on a set of 1000 repeated measurements for one specific strain point.

The resolution of the interrogator is set by the combined effect of all noise sources affecting our system (noise introduced by the broad band source, noise at the detectors of the IR camera, vibrations of the coupling fiber, etc.). Indeed, as shown in Fig. 4(d), fluctuations are observed in the peak position calculated using the CoG formula and corrected using the “correction” function on a set of 1000 repeated measurements for one specific strain point. Calculation of the standard deviation of the resulting signal allows estimating the resolution of the system around the specific FBG wavelength position. The same procedure can be repeated for all strain values within the calibration set, and its average value, which gives an indication about the resolution of the interrogator, turns out to be 2.5 pm.

### 4.3. Multiple FBGs Interrogation

The operating principle of the proposed devices allows simultaneous interrogation of multiple FBGs at the same time. Indeed, the total measurement range can be split in a series of non-overlapping measurement intervals. Each measurement interval is associated to one FBG and is processed independently. Clearly, with this approach there is a trade-off between the number of FBGs and the measurement range for each FBG: the product of these two must be less than or equal to the total measurement range (50 nm). Typically, for composite structures a strain measurement range of  $-5000 < \mu\epsilon < +5000$  is required. For our interrogator this translates into a minimum of five FBGs which can be simultaneously interrogated. In fact, monitoring of more than five FBGs can be envisaged in some practical applications, where the embedded FBGs are strained in the same direction during operation, as their peak reflected wavelengths will move accordingly, thus not overlapping.

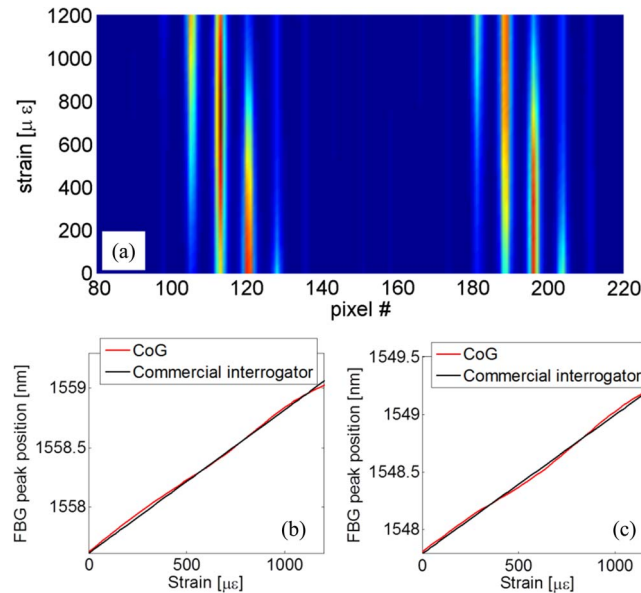


Fig. 5. Simultaneous measurement of two FBGs. (a) Evolution of the AWG response as a function of the applied strain. (b) and (c) FBG peak position estimated using the CoG (red line) and measured using the commercial interrogator (black line) as a function of the applied strain for the two sensors.

An example of simultaneous measurement of two FBGs (featuring peak reflections of  $-7$  dB around  $1547$  nm and  $1557$  nm, peak FWHM of  $120$  pm and strain sensitivity of  $7.8 \mu\text{m}^{-1} \times 10^{-7}$ ) is presented in Fig. 5. Two non-overlapping intervals are identified and processed independently. Same measurement accuracy as in the case of a single FBG is observed.

#### 4.4. Polarization Dependence of the Interrogator

The experiments reported so far have been performed on a device designed for TE polarization, featuring a 1-D grating coupler interface. As the 1-D grating coupler only couples the TE component of the input light onto the chip, no  $\text{PD}\lambda$  is present but a very large PDL is observed [see Fig. 7(a) and (b)]. For this reason, in the previous experiments, a polarization controller has been inserted before the PIC, which transforms the arbitrarily polarized signal reflected by the FBG into a TE polarized signal.

As the reflection from the FBG fiber typically will be randomly polarized, it is clear that for practical use of the proposed interrogator, a polarization handling scheme must be developed that allows reducing the PDL of the device to achieve a robustly detectable signal level at the output of the interrogator for any random status of the input polarization.

For this reason, as discussed in the introduction, two additional designs have been developed, which are variations of the original design, and feature a 2-D grating coupler as input interface to the PIC. The 2-D grating coupler [17] allows coupling both orthogonal input polarizations into the PIC, automatically splits them, and rotates one polarization by  $90^\circ$ . Thus, in the end, two TE polarized signals are available at the two output waveguides of the 2-D grating coupler.

The first design is based on a polarization diversity approach [see Fig. 6(a)]. The two orthogonal polarizations are processed independently by two identical replicas of the original design (the tailored AWG) and, unlike conventional polarization diversity approaches, the AWG outputs are not recombined using 2-D grating couplers, but 1-D grating couplers are used at the output of each identical AWG. Independently of the polarization status of the FBG reflection, an adequate signal level is always present at the output of one or both device replicas [see Fig. 7(c)–(f)], which allows to retrieve the FBG wavelength position. As both orthogonal polarizations are tracked

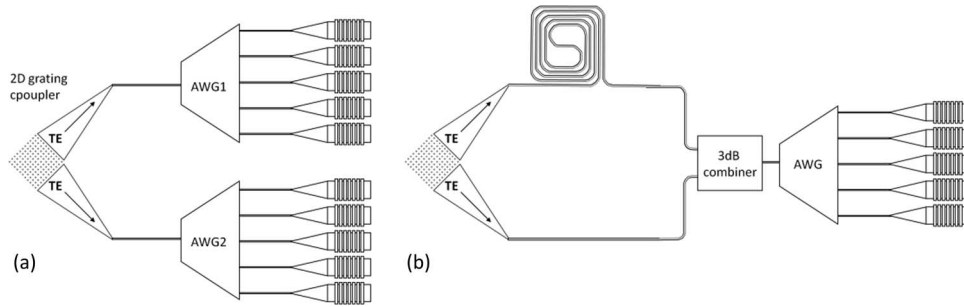


Fig. 6. Polarization independent schemes. (a) Polarization diversity approach. (b) Approach based on a Mach–Zehnder interferometer with one arm longer than the coherence length of the signal reflected by the FBG (and transmitted by the PIC).

simultaneously, this architecture has the additional advantage that multi-axial strain measurements are possible using Fiber Bragg Gratings inscribed in birefringent optical fibers [18].

The second proposed approach for polarization independent operation, is sketched in Fig. 6(b). In this case, the signal reflected by the FBG is first transmitted through a Mach–Zehnder interferometer composed by the input 2-D grating coupler and a 3 dB MMI combiner before being injected into the AWG. One of the two arms of the Mach–Zehnder is longer than the coherence length of the signal reflected by the FBG (and transmitted by the PIC).

Combinations of the two TE signals transmitted by the 2-D grating coupler would normally result in interference effects at the output of the 3 dB combiner due to the coherence between the two TE signals, thus the AWG would be fed with an impaired signal and proper operation of the device would be lost.

However, if one of the two TE signals transmitted by the 2-D grating is delayed by a path length longer than the coherence length of the input signal (transmitted by the PIC), no interference effects will be observed at the output of the 3 dB combiner. Thus, independently of the polarization status, the input signal is transformed into a TE signal albeit at the expense of an additional fixed 3 dB loss. The length of the delay path must be longer than the coherence length of the input signal (transmitted by the PIC). The coherence length  $L_c$  for a signal with spectral width  $\Delta\lambda$  is equal to

$$L_c = \frac{2\ln(2)}{\pi n} \frac{\lambda^2}{\Delta\lambda}. \quad (2)$$

As in our case the FBG peak has spectral width  $\Delta\lambda = 120$  pm (FWHM), the corresponding coherence length in the SOI optical waveguide is  $L_c \sim 3$  mm. This means that the longer delay arm can be reasonably integrated within the SOI PIC, and results in negligible additional propagation losses. The signal measured at the output of the device is presented in Fig. 7(g) and (h). Independently of the input polarization status, a proper signal can be detected and thus processed. No  $\text{PD}\lambda$  is present also in this case, and the measured PDL is reduced to only about 2 dB which makes the use of the device practical, as a detectable signal is produced at the output of the device for any arbitrary status of the reflected polarization. In addition to the simplicity and reduced footprint, this scheme has the advantage of being robust with respect to the unavoidable fabrication tolerances between the two identical AWG replicas in the case of the polarization diversity approach.

## 5. Conclusion

We reported on a novel FBG interrogator based on an optimized AWG filter, featuring large cross-talk between the channels, which allows simultaneous detection of multiple FBG

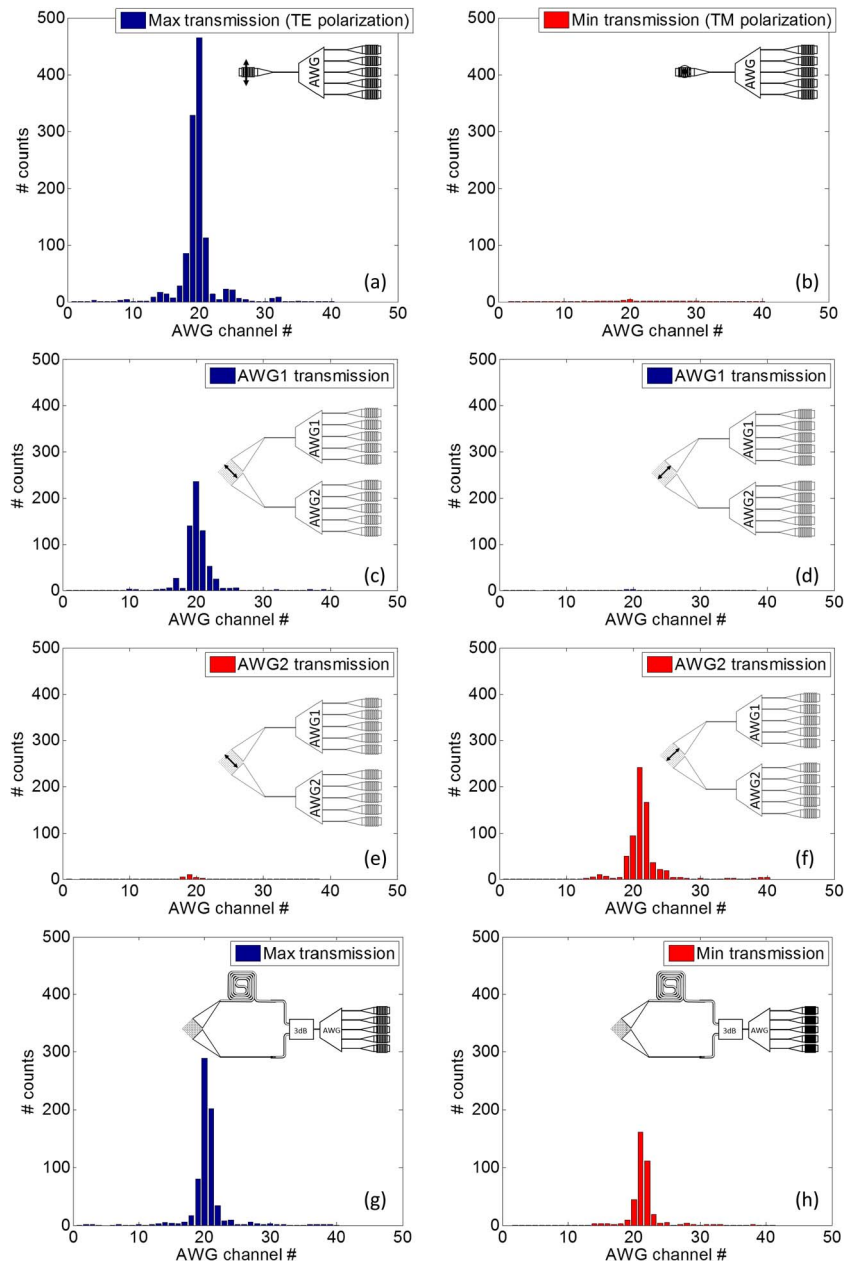


Fig. 7. Signal measured at the output of the different interrogator architectures for the same power of the FBG reflected signal. (a)–(b) Interrogator with 1-D input grating coupler. Operation is strongly polarization dependent. (c)–(f) Response of the interrogator featuring polarization diversity architecture for different polarization statuses specified in the insets. (g) and (h) Response of the interrogator based on a Mach–Zehnder interferometer with one arm longer than the coherence length of the signal reflected by the FBG (and transmitted by the PIC) for different polarization statuses (best and worst transmission cases).

peaks, using centroid signal processing techniques. The measured resolution is 2.5 pm and the total measurement range is 50 nm. The device fabricated in SOI has a footprint of only  $2.2 \times 1.5$  mm. Polarization independent operation of the device is demonstrated. Hybrid integration with a III-V detector array is foreseen in the future in order to demonstrate a fully integrated miniaturized FBG interrogator with improved resolution.

## References

- [1] G. Luyckx, E. Voet, N. Lammens, and J. Degrieck, "Strain measurements of composite laminates with embedded fibre Bragg gratings: Criticism and opportunities for research," *Sensors*, vol. 11, no. 1, pp. 384–408, Dec. 2010.
- [2] A. D. Kersey, "Interrogation and multiplexing techniques for fiber Bragg grating strain-sensors," in *Proc. SPIE*, 1993, vol. 2071, pp. 30–48.
- [3] M. Song, S. Yin, and P. B. Ruffin, "Fiber Bragg grating strain sensor demodulation with quadrature sampling of Mach-Zehnder interferometer," *Appl. Opt.*, vol. 39, no. 7, pp. 1106–1111, Mar. 2000.
- [4] A. D. Kersey *et al.*, "Fiber grating sensors," *J. Lightw. Technol.*, vol. 15, no. 8, pp. 1442–1463, Aug. 1997.
- [5] M. A. Davis and A. D. Kersey, "All-fiber Bragg grating strain-sensor de-modulation technique using a wavelength division coupler," *Electron. Lett.*, vol. 30, no. 1, pp. 75–77, Jan. 1994.
- [6] S. H. Yun, D. J. Richardson, and B. Y. Kim, "Interrogation of fiber grating sensor arrays with a wavelength-swept fiber laser," *Opt. Lett.*, vol. 23, no. 11, pp. 843–845, Jun. 1998.
- [7] Y. Sano and T. Yoshino, "Fast optical wavelength interrogator employing arrayed waveguide grating for distributed fiber Bragg grating sensors," *J. Lightw. Technol.*, vol. 21, no. 1, pp. 132–139, Jan. 2003.
- [8] P. Cheben *et al.*, "Tilted fiber Bragg grating sensor interrogation system using a high-resolution silicon-on-insulator arrayed waveguide grating," *Opt. Lett.*, vol. 33, no. 22, pp. 2647–2649, Nov. 2008.
- [9] D. C. C. Norman, D. J. Webb, and R. D. Pechstede, "Extended range interrogation of wavelength division multiplexed fiber Bragg grating sensors using arrayed waveguide grating," *Electron. Lett.*, vol. 39, no. 24, pp. 1714–1715, Nov. 2003.
- [10] P. Niewczas, A. J. Willshire, L. Dziuda, and J. R. McDonald, "Performance analysis of the fiber Bragg grating interrogation system based on an arrayed waveguide grating," *IEEE Trans. Instrum. Meas.*, vol. 53, no. 4, pp. 1192–1196, Aug. 2003.
- [11] D. C. C. Norman, D. J. Webb, and R. D. Pechstedt, "Interrogation of fibre Bragg grating sensors," *Meas. Sci. Technol.*, vol. 16, no. 3, pp. 691–698, Jan. 2005.
- [12] R. N. John, I. Read, and W. N. MacPherson, "Design considerations for a fibre Bragg grating interrogation system utilizing an arrayed waveguide grating for dynamic strain measurement," *Meas. Sci. Technol.*, vol. 24, no. 7, Jun. 2013, Art. ID 075203.
- [13] H. Fukuda *et al.*, "Silicon photonic circuit with polarization diversity," *Opt. Exp.*, vol. 16, no. 7, pp. 4872–4880, Mar. 2008.
- [14] T. Barwicz *et al.*, "Polarization-transparent microphotonic devices in the strong confinement limit," *Nat. Photon.*, vol. 1, no. 1, pp. 57–60, Jan. 2007.
- [15] J. Zhang *et al.*, "A tunable polarization diversity silicon photonics filter," *Opt. Exp.*, vol. 19, no. 14, pp. 13063–13072, Jul. 2011.
- [16] D. Dai and J. E. Bowers, "Novel concept for ultracompact polarization splitter-rotator based on silicon nanowires," *Opt. Exp.*, vol. 19, no. 11, pp. 10940–10949, May 2011.
- [17] H. Fukuda *et al.*, "Ultrasmall polarization splitter based on silicon wire waveguides," *Opt. Exp.*, vol. 14, no. 25, pp. 12401–12408, Dec. 2006.
- [18] D. Taillaert *et al.*, "A compact two-dimensional grating coupler used as a polarization splitter," *IEEE Photon. Technol. Lett.*, vol. 15, no. 9, pp. 1249–1251, Sep. 2003.
- [19] G. Luyckx *et al.*, "Response of FBGs in microstructured and bow tie fibers embedded in laminated composite," *IEEE Photon. Technol. Lett.*, vol. 21, no. 18, pp. 1290–1292, Sep. 15, 2009.
- [20] A. Othonos and K. Kalli, *Fiber Bragg Gratings: Fundamentals and Applications in Telecommunications and Sensing*. Boston, MA, USA: Artech House, 1999, pp. 301–388.
- [21] M. Smit and C. VanDam, "PHASAR-based WDM-devices: Principles, design and applications," *IEEE J. Sel. Topics Quantum Electron.*, vol. 2, no. 2, pp. 236–250, Jun. 1996.
- [22] S. Pathak, D. Van Thourhout, and W. Bogaerts, "Design trade-offs for silicon-on-insulator-based AWGs for (de)multiplexer applications," *Opt. Lett.*, vol. 38, no. 16, pp. 2961–2964, Aug. 2013.
- [23] W. Bogaerts *et al.*, "Compact wavelength-selective functions in silicon-on-insulator photonic wires," *IEEE J. Sel. Topics Quantum Electron.*, vol. 12, no. 6, pp. 1394–1401, Nov./Dec. 2006.
- [24] D. Taillaert *et al.*, "An out-of-plane grating coupler for efficient Butt-coupling between compact planar waveguides and single-mode fibers," *IEEE J. Quantum Electron.*, vol. 38, no. 7, pp. 949–955, Jul. 2002.